IJEMD-M, 1 (2) (2022), 11 - 22 https://doi.org/10.54938/ijemdm.2022.01.2.26

IJEMD

International Journal of Emerging Multidiciplinaries: Mathematics

Research Paper

Journal Homepage: www.ijemd.com

ISSN: 2790-1998 (print), 2790-3257 (online)

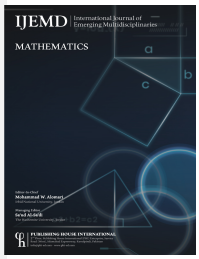

Numerical Analysis Of a Falling Circular Particle Passing through a Fluid Channel having Diamond Shaped Obstacles

Muhammad Majid[1], Nida Nazakat[1], Kamran Usman[1*] and Muhammad Shahid[1]

[1]*Department of Mathematics, Air University, Islamabad 44000, Pakistan*

[*]*Corresponding author*

Abstract

It has been analyzed that the particle motion inside a vertical channel while passing across diamond shaped obstacles produces severe effects on the fluid. Particle interaction with outer boundary, internal obstacles and with the fluid is inspected. An Eulerian based approach using a computational mesh is used in which solid particles are allowed to move freely in fluid domain. Fluid and particle interaction inside the whole domain is carried using Fictitious boundary method (FBM). A multigrid finite element method combined with the fictitious boundary method (FEM-FBM) is used for the simulation of in-compressible fluid flow along with rigid particle falling and colliding inside a fluid domain. A collision model to treat the Particle-obstacle and particle-wall interactions is used to avoid particle overlapping. The particulate flow is evaluated using an open source multigrid finite element solver FEATFLOW. Numerical investigations are executed in view of different particle positions and different alignment of diamond shaped obstacles. Effects on the movement of the particle and on the interaction of the fluid-particle system due to particle-wall, particle-Obstacle, particle-fluid interactivity has been analyzed.

Keywords: *Direct Numerical Simulation; Fictitious Boundary Method; Finite Element Method; Multigrid; Particulate Flow; Sedimentation.*

1. Introduction

A lot of natural and industrial processes are observed while examining solid particles in fluid for instance granular flows, sedimentation, particles cluster and multi-phase flows. Motion of particles in fluid covers a vast area of industrial applications such as grease transport, fluidized interruption, sedimentation, slurry flow, pulpwood, food processing etc. Many flows occur naturally in various phenomenon such as sand or dirt particles, lava flows and sedimentation in estuary etc.

In majority of cases, such particle interactions involve collisions with other particles and obstacles present inside the domain. Engineering applications of fluid-particle, fluid-wall boundaries can be found as hanging bridges, free-standing towers and high rise buildings inside the atmospheric air. A fundamental knowledge is lacking for the study of such particle interaction with obstacles inside the domain which results in different formations assisted by the particle interaction and collisions in modeling of particulate flows [39]. To inspect the rigid solid-liquid flows [40] various methodologies have been introduced during the last decade. Particulate flow phenomena is mainly modeled by two approaches, continuum and the discrete method approach. In continuum method, the mass of a particle is considered as a synthetic continuum and is constructed on the solution of the conservation equations which works specifically for flow regimes [1]. Rapid granular flow and slow granular flow concepts have been successfully presented by Chapman, Ogawa and Rao et al. [1]. Currently, Sokolov and coauthors [2] have utilized a volume set methodology for the solution of PDE's combined with generalizations of Euclidean spaces and surfaces. The method focuses on the discrete approach that takes into account the shifting of particle inside a domain. The interaction of all the particles with one another and with their moving conditions is modeled

Email addresses: **mmajidiui@gmail.com (M. Majid), hozaifakhan.566@gmail.com (N. Nazakat), kamran.usman@mail.au.edu.pk (K. Usman), mshahidch@outlook.com (M. Shahid)**

in this method which is followed by calculating their trajectories, directions and spins [3]. A vast range of industrial occurrences have been examined using $(2D)$ and $(3D)$ DEM simulations [4, 41].

To predict the behavior of particulate flow with internal obstacles, a basic but thorough knowledge of particle-obstacle and particle-wall collisions is needed. Particle-particle interactions have been concluded in recent studies at low Reynolds numbers. Classical lubrication theory suggests that when particle boundaries reach very near to each other then the lubrication force between them becomes singular and thus avoids the particles from touching. Lubrication forces are introduced in lattice Boltzmann simulations [24] and stokes multiple simulations [25] when solid particles are approaching each other or are nearly in contact. Brady and Bossis [25] have considered stokes flow assumption using the stokesian dynamic techniques and have simulated the particulate flow with it. The discrete method is mainly classified into two approaches for the simulation of particulate flow, (a) the Eulerian approach (b) the Lagrangian approach. Joseph and Glowinski proposed a similar technique [5] based on this approach. The Lagrangian approach can be defined on the concept of moving course mesh nodes which moves along with the motion of particle wall. A reconstruction of this approach is Arbitrary Lagrangian Eulerian Approach (ALE) [6, 7, 8]. In Eulerian approach the course mesh nodes are fixed at their initial positions which is suitable for a low computational cost with sufficient numerical estimates.

In this method which is proposed by Glowinski and Singh [9, 10], FEM background carries the rigid particles inside the fluid channel using an Eulerian approach where rigid particles are handled individually through Newton-Euler equations. On the other hand, computational grid is altered in ALE technique near the fluid and particle interface and the process is moved forward with the Lagrangian motion of the new replaced mesh nodes. A particular treatment of such method is the distributed Lagrange multiplier method (DLM) coupled with the fictitious boundary method [16, 17, 18, 39] developed by Glowinski [5, 9, 42, 43]. Patankar et al. [6, 19] introduced a stress field in the particle domain and merged it with the DLM method to get rid of the necessity to determine particle's translational velocity. Abbasi et al. [21] analyzed the phenomenon when multiple structures are in wake of one another, the mechanism depends upon the adjustment, gap distance, shape and size of structures. Inoue et al.[22] implanted a technique based on finite difference method in order to find the solution of 2D unsteady compressible Navier-Stokes equation and analyzed the wake achieved by two square obstacles arranged on staggered positions by considering space effect between them in a uniform flow at low Mach numbers. Wang et al.[23] considered computational mesh as a horizontal soap film tunnel along with two circular obstacles placed in staggered positions.

In order to prevent the complicated collisions of the particles with each other, channel wall and internal obstacles, a true definition for the collision model [26] is needed because collision or near collision of the solid rigid particles can cause extreme problems in case the rigid particles are very close to each other and thus remarkably increase the evaluation and cost of simulation [27]. Recently, Usman [28] presented a brief comparison of distinct collision models for circular rigid particles in a two dimensional framework in fluid channel. In other observations, researchers have concluded that for rough particles, physical touching might happen which may consequently effect the dependent motion of the rigid solid particles [29]. Ardekani and Rangel [30] used distributed Lagrange multiplier approach to simulate unsteady motion and collision of two particles in fluid having a dilute suspension with control volume approach [31]. A simple algorithm to simulate colliding particles has been discussed by Patankar [32].

The current study is to find the numerical behavior of falling rigid particle colliding and passing near diamond shaped internal obstacles and interacting with the boundary of the domain in a fluid channel. The computational mesh is chosen with an Eulerian based method which is fixed and is independent of the particle structure and dimensions. To control particle collisions, in case of colliding with internal obstacles and with the wall of the channel, collision models are used to intercept this interacting process. We have defined particle-cylinder collision model and particle-wall collision model for particle interactions with diamond shaped obstacles and collision of particle with wall.

2. Mathematical Modeling

Consider fluid flow along with a solid particle having mass M_s and density ρ_s. ρ_f is the fluid density and ν represents the fluid viscosity. The domain occupied by the fluid is Ω_f and the domain occupied by the particle is Ω_s and $\partial\Omega_s$ represents boundary of the particle. Hence, the total domain is given by $\Omega_T = \Omega_f \cup \Omega_s$

2.1. Incompressible Fluid and Particle Motion

The motion of incompressible fluid in the domain Ω_f is governed by the Navier-Stokes equations [34]

$$\rho_f \left(\frac{\partial \boldsymbol{u}}{\partial t} + \boldsymbol{u} \cdot \nabla \boldsymbol{u} \right) - \nabla \cdot \sigma = 0, \quad \nabla \cdot \boldsymbol{u} = 0 \quad \forall t \in (0,T), \tag{2.1}$$

where σ is the total stress tensor in the fluid phase, defined as,

$$\sigma = -p\boldsymbol{I} + \mu_f \left[\nabla \boldsymbol{u} + (\nabla \boldsymbol{u})^T \right]. \tag{2.2}$$

Here, fluid velocity is $\boldsymbol{u}$, p is the pressure, coefficient of viscosity is μ_f and $\boldsymbol{I}$ is the identity tensor.
The translational and rotational motion of the freely moving rigid particle in fluid is due to the hydrodynamic forces, collision forces due to particle and outer wall and particle-cylinder interaction and gravitational acceleration. The Newton-Euler equations, in this case, takes the form

$$M_s \frac{d\boldsymbol{U}_s}{dt} = (\triangle M_s)\,\boldsymbol{g} + \boldsymbol{F}_s + \boldsymbol{F}'_s, \qquad \boldsymbol{I}_s \frac{d\omega_s}{dt} + \omega_s \times (\boldsymbol{I}_s \omega_s) = \boldsymbol{T}_s. \tag{2.3}$$

$\boldsymbol{U}_s$ and ω_s respectively are the translational and angular velocities of the particle, M_s is the particle mass and we write $\triangle M_s = M_s - M_f$, where M_f is the mass occupied by the fluid in the same volume as M_s. Drag and lift forces acting on the particle are represented by $\boldsymbol{F}_s$, $\boldsymbol{F}'_s$ are the particle collision forces, the moment of inertia tensor and the resultant torque acting about the center of mass of the particle is $\boldsymbol{I}_s$ and $\boldsymbol{T}_s$ respectively and $\boldsymbol{g}$ denotes the gravitational acceleration.
The position $\boldsymbol{X}_s$ of the center of mass of the particle and its angle θ_s can be obtained after integrating the following kinematic equations [35], [36],

$$\frac{d\boldsymbol{X}_s}{dt} = \boldsymbol{U}_s, \qquad \frac{d\theta_s}{dt} = \omega_s. \tag{2.4}$$

2.2. Drag and Lift Hydrodynamic Forces and Torque

The drag and lift forces $\boldsymbol{F}_s$ and the torque $\boldsymbol{T}_s$ acting on the mass center of the particle can be obtained by [37]

$$\boldsymbol{F}_s = (-1) \int_{\partial\Omega_s} (\sigma.\boldsymbol{n}) d\Gamma_s, \qquad \boldsymbol{T}_s = (-1) \int_{\partial\Omega_s} (\boldsymbol{X} - \boldsymbol{X}_s) \times (\sigma \cdot \boldsymbol{n})\, d\Gamma_s. \tag{2.5}$$

where the unit vector $\boldsymbol{n}$ acts normal to the boundary $\partial\Omega_s$ of the particle. Once the drag force is calculated, the drag and lift coefficients can be found using

$$C_d = \frac{2F_D}{\rho U^2 D}, \quad C_l = \frac{2F_L}{\rho U^2 D}, \tag{2.6}$$

where U and D is the characteristic velocity and length respectively.

2.3. Fluid-Particle Coupling using Fictitious Boundary Method

At the fluid and particle interface $\partial\Omega_s$, no-slip boundary conditions are applied and the velocity $\boldsymbol{u}_s(\boldsymbol{X})\ \forall\, \boldsymbol{X} \in \overline{\Omega}_s$ is given by,

$$\boldsymbol{u}_s(\boldsymbol{X}) = \boldsymbol{U}_s + \omega_s \times (\boldsymbol{X} - \boldsymbol{X}_s). \tag{2.7}$$

The fictitious boundary method (FBM) works over a multigrid finite element method by incorporating the particle domain within the fluid domain. The additional constraints arising due to the particle's boundary motion at the particle-fluid interface are included in the Navier-Stokes equations, by extending the fluid domain with the combined fluid and particle domain, which takes the form,

$$\begin{cases} \nabla.\boldsymbol{u} = 0 & \forall X \in \Omega_T \\ \rho_f(\frac{\partial \boldsymbol{u}}{\partial t} + \boldsymbol{u}.\nabla\boldsymbol{u}) - \nabla.\sigma = 0 & \forall X \in \Omega_f \\ \boldsymbol{u}(\boldsymbol{X}) = \boldsymbol{U}_s + \omega_s \times (\boldsymbol{X} - \boldsymbol{X}_s) & \forall X \in \overline{\Omega}_s. \end{cases} \tag{2.8}$$

2.4. Particle Collisions

We will use a collision model for the calculation of particle-wall collision forces F_s^W presented by Glowinski, Joseph, Singh and coauthors [10] and present a modified model for the particle-cylinder collision forces F_s^c. Therefore, $\boldsymbol{F}'_s = \boldsymbol{F}_s^c + \boldsymbol{F}_s^W$.

Particle-Cylinder Collision Model

We have introduced a small change in the collision model for interacting particle and cylinder proposed in [10], that is, we have considered the circular cylinder as a second particle and hence the model takes the form

$$\boldsymbol{F}_s^c = \begin{cases} 0, & for \quad D_{s,c} > R_s + R_c + \rho, \\ \frac{1}{\varepsilon_p}(\boldsymbol{X}_s - \boldsymbol{X}_c)(R_s + R_c + \rho - D_{s,c})^2, & for \quad R_s + R_c \le D_{s,c} \le R_s + R_c + \rho, \\ \frac{1}{\varepsilon'_p}(\boldsymbol{X}_s - \boldsymbol{X}_c)(R_s + R_c - D_{s,c}), & for \quad D_{s,c} \le R_s + R_c \end{cases} \tag{2.9}$$

the coordinates of the center of the cylinder are $\boldsymbol{X}_c$ and R_s and R_c denotes the radius of particle and cylinder respectively. The distance between $\boldsymbol{X}_s$ and $\boldsymbol{X}_c$ is $D_{s,c} = |\boldsymbol{X}_s - \boldsymbol{X}_c|$. ρ is the minimum distance to activate the force of repulsion between particle and cylinder and is taken one mesh element apart. Values for the positive stiffness parameters ε_p and ε'_p are chosen as such to avoid discontinuity or singularity.

Particle-Wall Collision Model

For particle-wall collision model, the corresponding model is expressed by [10]

$$\boldsymbol{F}_s^W = \begin{cases} 0, & for \quad D'_s > 2R_s + \rho, \\ \frac{1}{\varepsilon_\omega}\left(\boldsymbol{X}_s - \boldsymbol{X}'_s\right)\left(2R_s + \rho - D'_s\right)^2, & for \quad 2R_s \le D'_s \le 2R_s + \rho, \\ \frac{1}{\varepsilon'_\omega}\left(\boldsymbol{X}_s - \boldsymbol{X}'_s\right)\left(2R_s - D'_s\right), & for \quad D'_s \le 2R_s \end{cases} \tag{2.10}$$

where $\boldsymbol{X}'_s$ is the coordinate of the center of mass of the nearest imaginary particle p'_s imagined on the boundary wall with respect to the particle. $D'_s = |\boldsymbol{X}_s - \boldsymbol{X}'_s|$ is the distance between the center of the imaginary particle p'_s and the mass center of particle. ε_w and ε'_w are small positive stiffness parameters for particle-wall collisions, usually their values can be taken as $\varepsilon_w = \dfrac{\varepsilon_p}{2}$ and $\varepsilon'_w = \dfrac{\varepsilon'_p}{2}$ in the calculations.

3. Numerical Results

Behavior of a falling particle inside a vertical channel passing across four internal diamond shaped obstacleshas been examined. The falling particle disturbs the pressure field and consequently disturbs the fluid motion as well as the hydrodynamic forces (drag and lift forces) acting on the surface of Obstacles while it crosses the Obstacles. The disturbance propagates further towards the following obstacles while particle passes across the obstacles and results in different patterns for fluid and particle motion. The collisions and near-overlapping of particle with obstacles and with the outer wall are averted using collision models discussed in equation (2.9) and equation (2.10). The dimension of the fluid domain is 15 and 3 along y-axis and x-axis respectively as shown in figure 3.1. The falling rigid 2D particle has density $\rho_s = 1.25$. Density of in-compressible fluid is taken $\rho_f = 1.0$ and the Reynolds number is $Re = 100$. In all the numerical simulations we consider the particle of radius $R = 0.25$. We have considered that initially at $t = 0$ the fluid and particle are both at rest. The gravitational acceleration $\boldsymbol{g} = 980$ is the only force to start the falling motion of the particle. Zero dirichlet boundary conditions at the walls of the fluid channel are assumed. The simulations are carried out on fixed computational meshes by using CFD code FEATFLOW [38]. Moreover, the effect of spacing between different Obstacles is also numerically studied by increasing their internal gap and moving the second and fourth Obstacle at different positions. Numerical simulations are executed on mesh refinement level-5 comprising of $81,920$ number of elements in such a way that mesh independence is guaranteed at this refinement level. The experiments are

performed keeping three different initial positions of the particle in x-direction while retaining the same y-position. In the first basic case, diamond shaped obstacles are placed at positions $(1.5,12)$,$(1.5,9)$,$(1.5,6)$ and $(1.5,3)$ whereas a variety of configurations for the position of obstacle are selected comprising of inline Obstacles and staggered obstacles with each other. Moreover, the study includes effect of moving second obstacle in negative x-direction and fourth Obstacle in y-direction at three different positions.

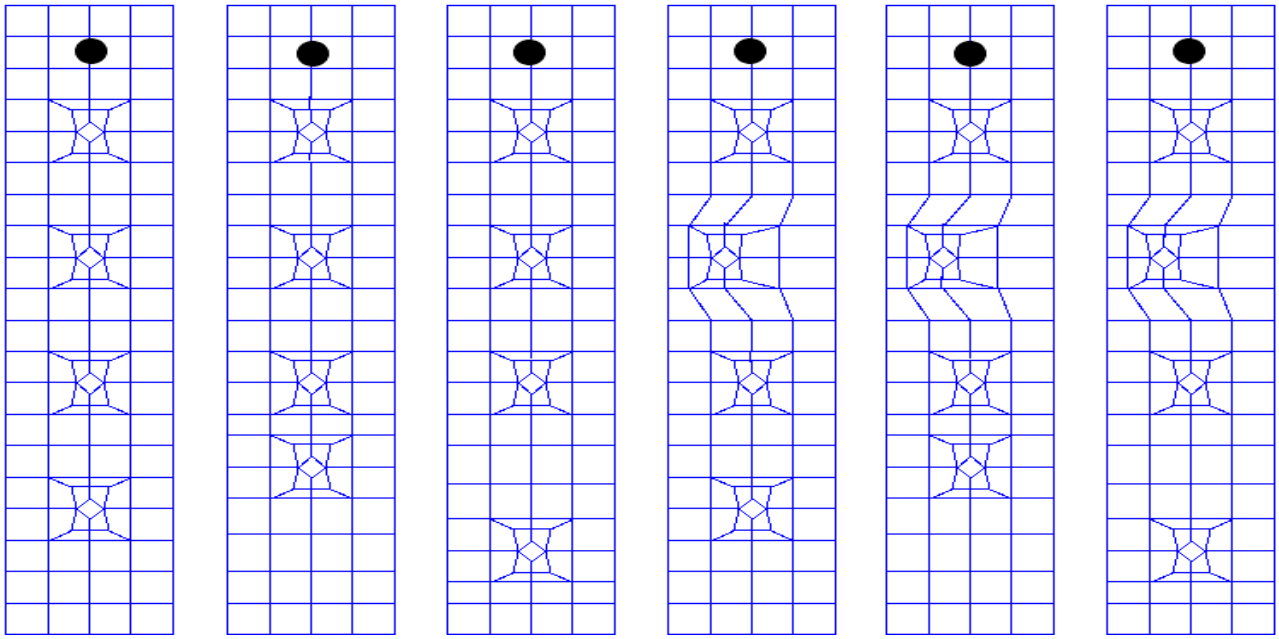

(a) Case1 **(b)** Case2 **(c)** Case3 **(d)** Case4 **(e)** Case5 **(f)** case6

Figure 3.1: schematic of different course meshes with obstacles and particle

Images in figure 3.1 show the different position of diamond shaped obstacles and particle. Different images show the position of particle at different times and the effect of particle on fluid motion and its behavior. Fig 3.1 shows coarse meshes and using these meshes we have numerically performed all the simulations on these meshes with different configurations of the obstacle and particle position. Snapshots of some selected cases are presented in the study but complete cases are discussed using tables. These are total 18 cases in which we have found all the numerical results and simulations are performed with obstacles placed in inline and staggered positions which are as follows:

(i) $(1.5,12.0)$,$(1.5,9.0)$,$(1.5,6.0)$, $(1.5,3.0)$ (ii) $(1.5,12.0)$,$(1.5,9.0)$,$(1.5,6.0)$,$(1.5,4.0)$
(iii) $(1.5,12.0)$,$(1.5,9.0)$,$(1.5,6.0)$,$(1.5,2.0)$ (iv) $(1.5,12.0)$,$(1.0,9.0)$,$(1.5,6.0)$,$(1.5,3.0)$
(v) $(1.5,12.0)$,$(1.0,9.0)$,$(1.5,6.0)$,$(1.5,4.0)$ (vi) $(1.5,12.0)$,$(1.0,9.0)$,$(1.5,6.0)$,$(1.5,2.0)$

Figure 3.2(a) to 3.2(f) shows four obstacles placed in an inline arrangement. The first obstacle C_1 is placed at position $(1.5,12)$ and C_2 is at position $(1.5,9)$. The third obstacle C_3 is placed at position $(1.5,6)$ and fourth Obstacle C_4 is at position $(1.5,2)$ while the falling position of particle is $(1.80,14)$ inside a fluid channel. In figures 3.2(a) to 3.2(f), particle is shown colliding and passing from right side of the obstacles.

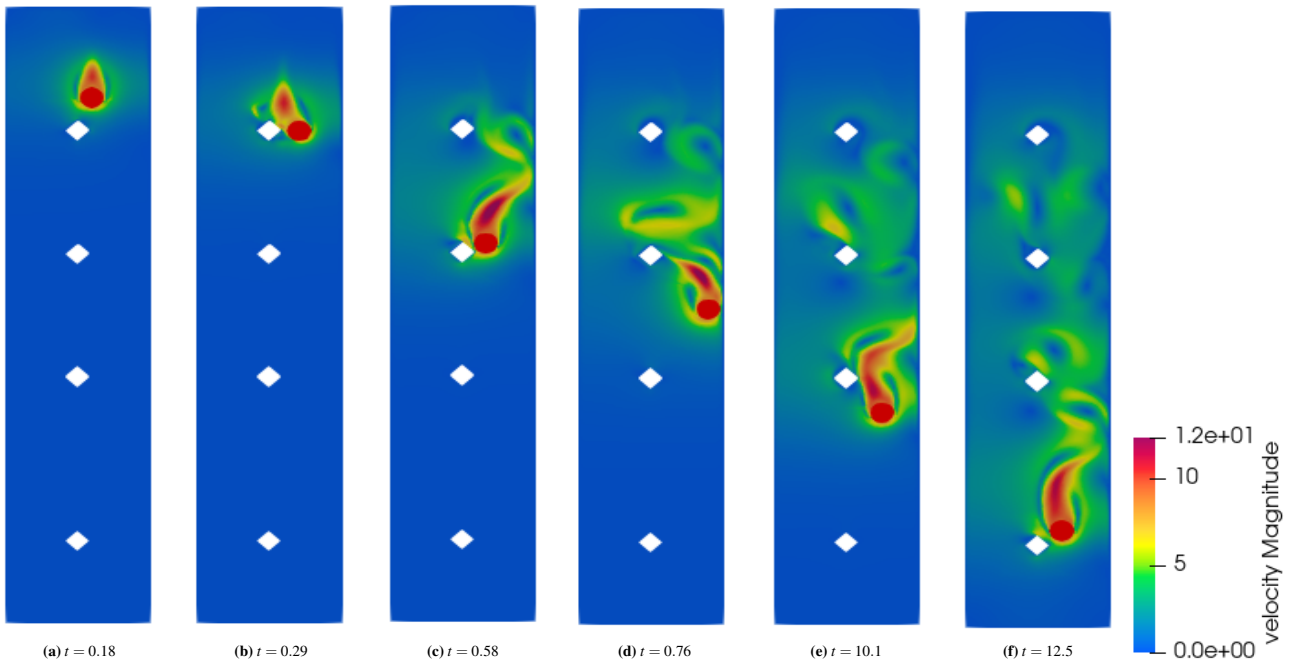

(a) $t = 0.18$ (b) $t = 0.29$ (c) $t = 0.58$ (d) $t = 0.76$ (e) $t = 10.1$ (f) $t = 12.5$

Figure 3.2: Snapshots of falling particle at different time steps

Different images in figure 3.2 show the position of particle at different time and the disturbance it creates while falling down and crossing the obstacles.

3.1. Trajectories

Now we present the trajectories of a falling particle while colliding and passing across the inner diamond shaped obstacles. Trajectories represents the path of the falling particle in a fluid channel while crossing the obstacles. The figures of trajectories show that rigid particle falls either from the right side or the left side of the obstacles. In fig 3.3(a), obstacles are in inlined formation while in fig 3.3(b-f), obstacles are placed in a staggered formation.

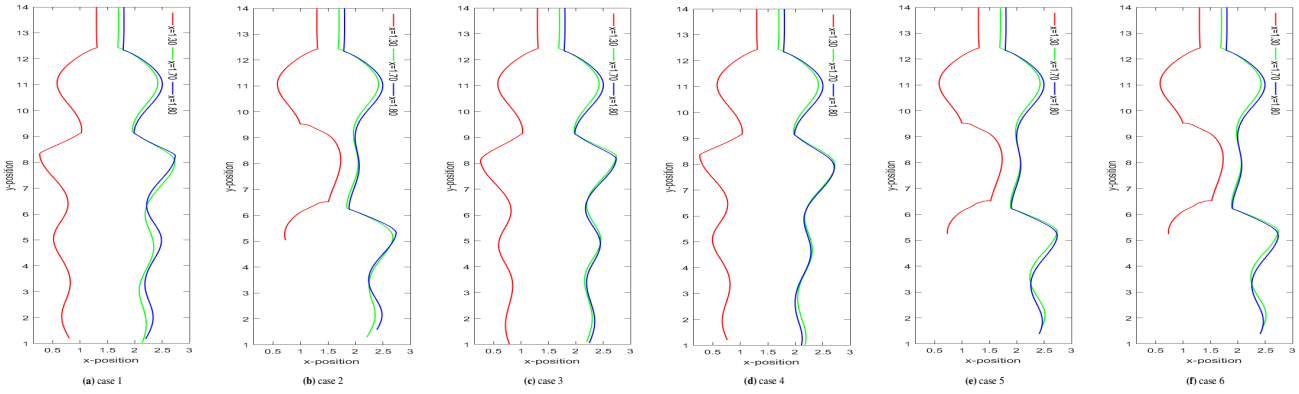

(a) case 1 (b) case 2 (c) case 3 (d) case 4 (e) case 5 (f) case 6

Figure 3.3: Trajectories of particle with different starting positions

We denote by C_1, C_2, C_3 and C_4 the first, second, third and fourth obstacles respectively. Similarly, we will denote C_{1x} and C_{2x} for the x-position of the first and second Obstacle. In each case C_1 and C_3 are fixed at position $(1.5, 12)$ and $(1.5, 6)$ respectively while obstacle C_2 is set on two different positions $(1.5, 9)$ and $(1, 9)$. In a similar fashion, C_4 is set on three different positions $(1.5, 3)$,$(1.5, 4)$ and $(1.5, 2)$. Figure 3.3(a)shows results when obstacles are in an inline position i.e. the first Obstacle C_1 is at position $(1.5, 12)$, second obstacle C_2 is at position $(1.5, 9)$, third obstacle C_3 is at position $(1.5, 6)$ and fourth Obstacle C_4 is at position $(1.5, 3)$. The simulations are performed by taking three particle starting positions $(1.30, 14)$, $(1.70, 14)$ and $(1.80, 14)$ as shown in red, green and blue lines respectively. When the starting position of the particle is $(1.30, 14)$, it passes from left of the obstacles while colliding and interacting with the obstacles. For the other two starting positions, the particle passes from right side of the obstacles. It has been concluded that the starting position of the particle, gap between the obstacles and the arrangement of obstacles (inline or staggered) have a deep impact on the fluid motion and suggest various paths for the

particles movement. Such as in figure 3.3(c) the red line shows that particle passes through the left side of the obstacles, green and blue lines show that the particle passes the obstacles from left side. In figures 3.3(a) to 3.3(f), the trajectories of particle are shown with internal diamond shaped obstacles having inline and staggered arrangements. In these figures red, green and blue colors represent the falling positions of particle $(1.30, 14)$,$(1.70, 14)$ and $(1.80, 14)$ respectively.

3.2. Drag and Lift coefficients on diamond shaped obstacles

We have presented the fluctuation in drag coefficient under different scenarios of obstacle arrangements. These scenarios consists of various initial positions of the particle, position of obstacles and the gap between obstacles. The oscillations represented by graphs in figure 3.4 show drag coefficients calculated on obstacles C_1, C_2 and C_3. Figure 3.4a shows graph of drag coefficient on obstacle C_1, figure 3.4b shows the graph of drag coefficient on obstacle C_2 and figure 3.4c shows the graph of drag on Obstacle C_3. The graph shows that the drag value instantly shoots up to a very high value when the particles comes in contact or crosses the obstacle C_1, C_2 and C_3, and gradually reaches its mean value after crossing the obstacle. Some selected cases for different configurations of obstacles have been shown in the graphs.

Figure 3.4 shows result for the case (i) when obstacle C_1, C_2 and C_3 are inline at positions $(1.5, 12)$, $(1.5, 9)$ and $(1.5, 6)$ respectively and particle's starting position is $(1.30, 14)$.

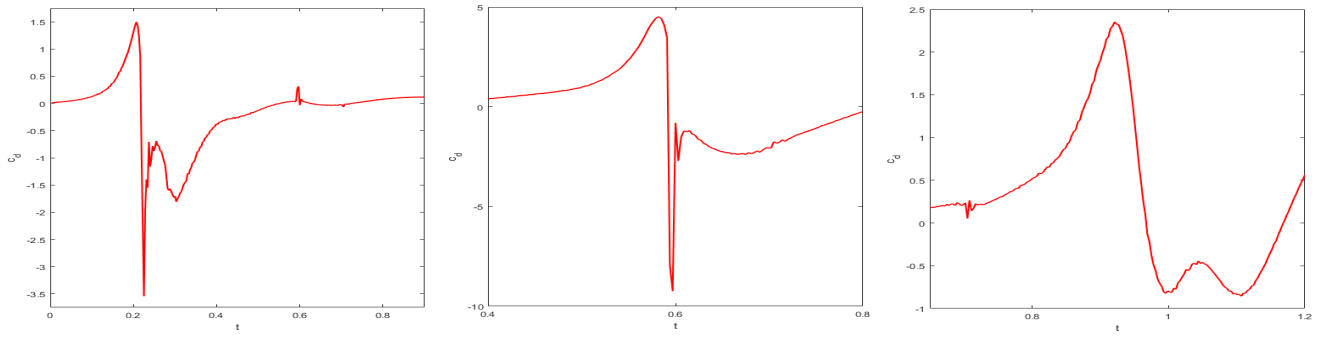

(a) Drag on C_1 **(b)** Drag on C_2 **(c)** Drag on C_3

Figure 3.4: *case*(i), Particle position=$(1.30, 14.0)$

Figure 3.5 shows result for the case (ii) in which obstacles C_1, C_2 and C_3 are inline at positions $(1.5, 12)$, $(1.5, 9)$ and $(1.5, 6)$ respectively with particle starting position $(1.70, 14)$. In fig 3.5a, fig 3.5b and fig 3.5c, graphs of drag on C_1, C_2 and C_3 are shown respectively.

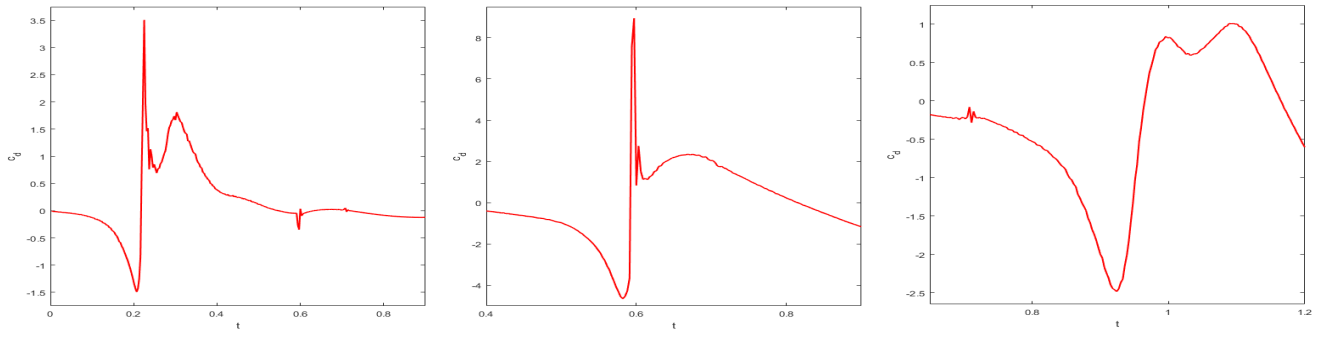

(a) Drag on C_1 **(b)** Drag on C_2 **(c)** Drag on C_3

Figure 3.5: *case*(ii), Particle position=$(1.70, 14.0)$

Figure 3.6 shows result for the case (iii) in which obstacles C_1, C_2 and C_3 are inline at positions $(1.5, 12)$, $(1.5, 9)$ and $(1.5, 6)$ respectively with particle starting position $(1.80, 14)$.

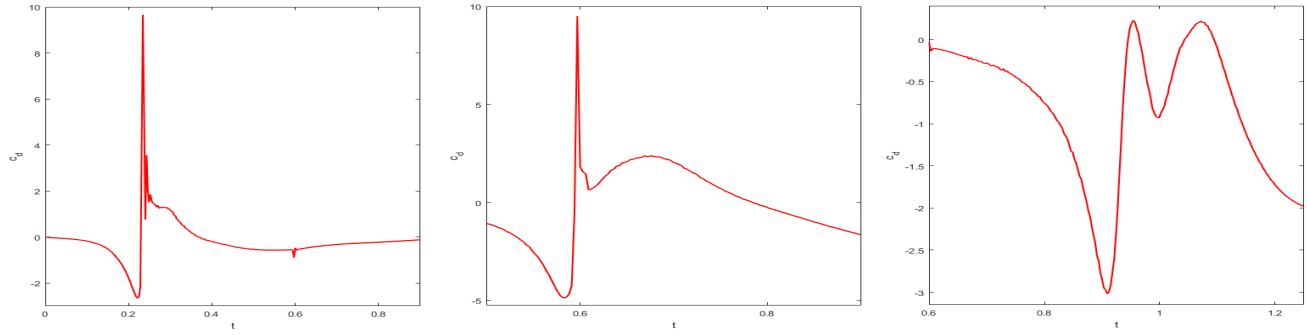

(a) Drag on C_1 **(b)** Drag on C_2 **(c)** Drag on C_3

Figure 3.6: *case*(iii), Particle position=$(1.80, 14)$

Figure 3.7 shows result for the case (iv) in which obstacles C_1, C_2 and C_3 are arranged in a staggered position at $(1.5, 12)$, $(1.0, 9)$ and $(1.5, 6)$ respectively along with the particle starting position $(1.30, 14)$.

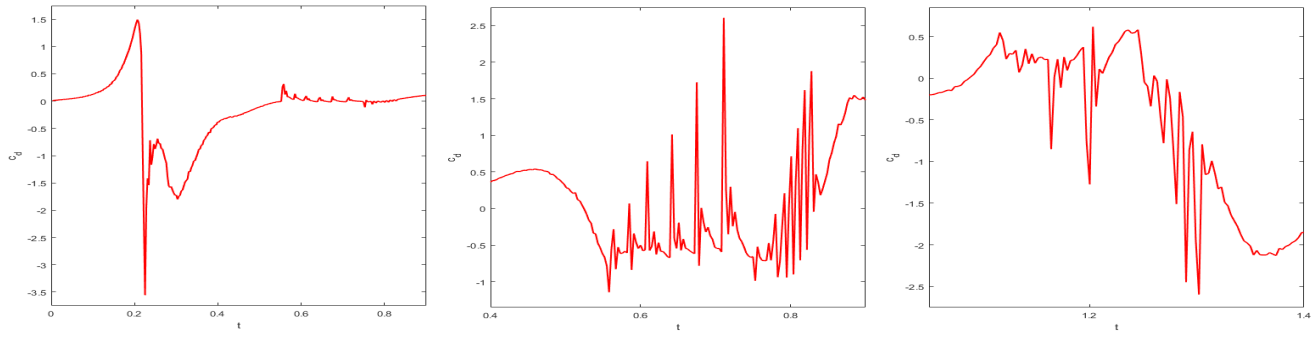

(a) Drag on C_1 **(b)** Drag on C_2 **(c)** Drag on C_3

Figure 3.7: *case*(iv), Particle position=$(1.30, 14)$

Figure 3.8 shows result for the case (v) in which obstacles C_1, C_2 and C_3 are placed in staggered positions at $(1.5, 12)$, $(1.0, 9)$ and $(1.5, 6)$ with particle starting position $(1.70, 14)$.

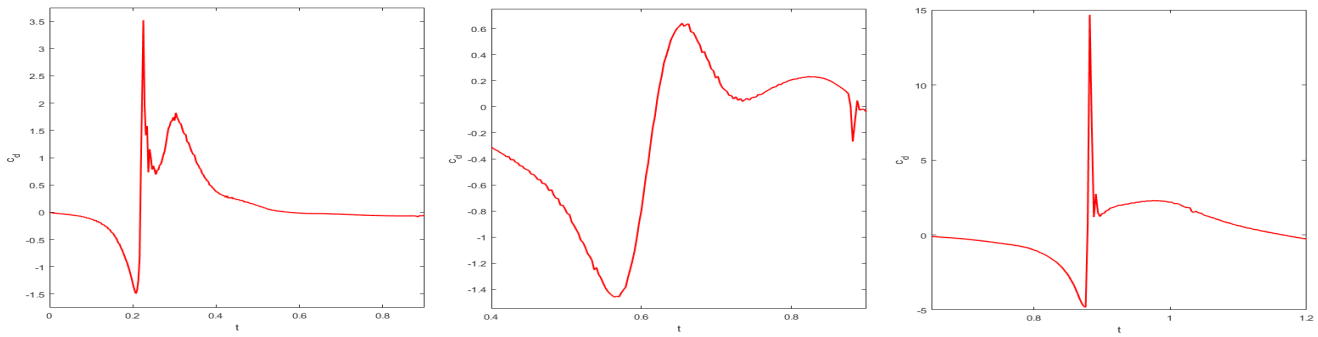

(a) Drag on C_1 **(b)** Drag on C_2 **(c)** Drag on C_3

Figure 3.8: *case*(v), Particle position=$(1.70, 14)$

Figure 3.9 shows result for the case (vi) in which obstacles C_1, C_2 and C_3 are staggered at positions $(1.5, 12)$, $(1.0, 9)$ and $(1.5, 6)$ with particle starting position $(1.80, 14)$.

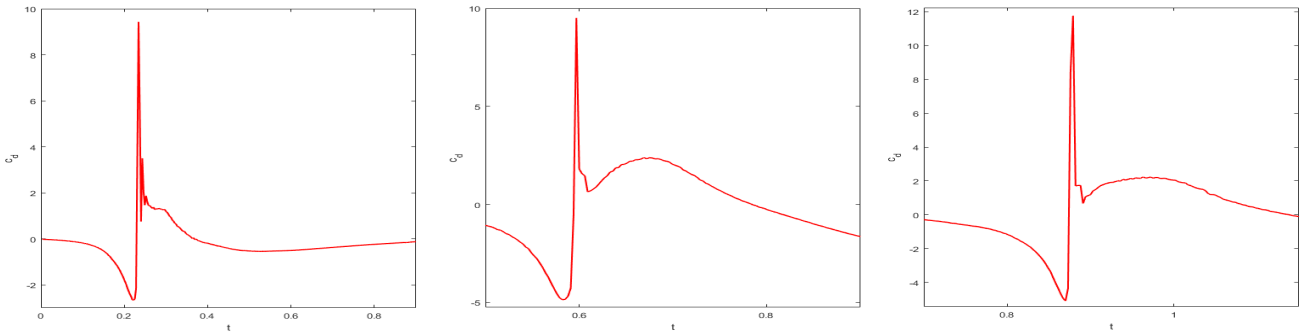

(a) Drag on C_1 **(b)** Drag on C_2 **(c)** Drag on C_3

Figure 3.9: $case(vi)$, Particle position=$(1.80, 14)$

3.3. Max/min drag value, time to cross obstacles and x-Shifts by particle

The drag values on obstacles C_2 and C_3 changes rapidly as soon as the particle reaches near the obstacle and starts crossing it. The drag values are more extreme if the particle passes by the obstacle while touching or colliding with it as shown in table 1, table 2, table 3, table 4, table 5 and table 6.

Table 1: Case (i): Time to cross obstacles, shifts and drag coefficient

Particle Position	C_d on C_2		C_d on C_3		t_2	t_4
	min	max	min	max		
1.30	-1.1566	2.5724	-3.1146	1.3187	0.186	0.105
1.70	-1.4575	0.6410	-4.7965	14.0455	0.099	0.105
1.80	-1.4186	0.4447	-5.1015	11.7693	0.099	0.099

Particle Position	S_2		S_3		S_4	
	min	max	min	max	min	max
1.30	0.4023	—	0.5915	—	0.7132	—
1.70	—	2.4925	—	2.2556	—	2.1322
1.80	—	2.5317	—	2.3959	—	2.2828

Table 2: Case (ii): Time to cross obstacles, shifts and drag coefficient

Particle Position	C_d on C_2		C_d on C_3		t_2	t_4
	min	max	min	max		
1.30	-8.5243	4.615	-0.8544	2.8319	0.114	0.096
1.70	-4.6552	8.9458	-2.4851	1.0109	0.117	0.096
1.80	-5.0050	11.209	-2.7978	0.9981	0.096	0.096

Particle Position	S_2		S_3		S_4	
	min	max	min	max	min	max
1.30	0.4857	—	0.7062	—	0.6262	—
1.70	—	2.5692	—	2.3755	—	2.3630
1.80	—	2.5072	—	2.3302	—	2.4009

Table 3: Case (iii): Time to cross obstacles, shifts and drag coefficient

Particle Position	C_d on C_2		C_d on C_3		t_2	t_4
	min	max	min	max		
1.30	-11.9968	4.6287	-0.85815	2.2524	0.123	0.096
1.70	-4.5313	8.9161	-2.9473	0.4273	0.111	0.093
1.80	-4.8605	9.5039	-3.0186	0.22557	0.108	0.093

Particle Position	S_2		S_3		S_4	
	min	max	min	max	min	max
1.30	0.3980	—	0.5643	—	0.6740	—
1.70	—	2.4716	—	2.2531	—	2.1849
1.80	—	2.4183	—	2.2679	—	2.1124

Table 4: Case (iv): Time to cross obstacles, shifts and drag coefficient

Particle Position	C_d on C_2		t_3	S_3		S_4	
	min	max		min	max	min	max
2.48	-4.6583	0.9680	0.081	—	2.5555	—	2.5698
2.55	-4.6711	1.2596	0.081	—	2.5544	—	2.5428
2.62	-3.7473	2.0074	0.081	—	2.6514	—	2.6162

Table 5: Case (v): Time to cross obstacles, shifts and drag coefficient

Particle Position	C_d on C_2		t_3	S_3		S_4	
	min	max		min	max	min	max
2.48	-4.6560	0.9691	0.081	—	2.5558	—	2.6072
2.55	-4.6797	1.2598	0.081	—	2.5532	—	2.5761
2.62	-3.7491	2.0163	0.081	—	2.6504	—	2.6174

Table 6: Case (vi): Time to cross obstacles, shifts and drag coefficient

Particle Position	C_d on C_2		t_3	S_3		S_4	
	min	max		min	max	min	max
2.48	-4.6560	0.9691	0.081	—	2.5558	—	2.6072
2.55	-4.6797	1.2598	0.081	—	2.5532	—	2.5761
2.62	-3.7491	2.0163	0.081	—	2.6504	—	2.6174

Table 1 shows simulations performed keeping case (i) and using three particle starting positions $(1.30, 14.0)$, $(1.70, 14.0)$ and $(1.80, 14.0)$. Table 2 shows simulations performed keeping case (ii) and using three particle starting positions $(1.30, 14.0)$, $(1.70, 14.0)$ and $(1.80, 14.0)$. Table 3 shows simulations performed keeping case (iii) and using three particle starting positions $(1.30, 14.0)$, $(1.70, 14.0)$ and $(1.80, 14.0)$. Table 4 shows simulations performed keeping case (iv) and using three particle starting positions $(1.30, 14.0)$, $(1.70, 14.0)$ and $(1.80, 14.0)$. Table 5 shows simulations performed keeping case (v) and using three particle starting positions $(1.30, 14.0)$, $(1.70, 14.0)$ and $(1.80, 14.0)$. Table 6 shows simulations performed keeping case (vi) and using three particle starting positions $(1.30, 14.0)$, $(1.70, 14.0)$ and $(1.80, 14.0)$. The table shows maximum drag value or minimum drag value on obstacle C_2 and obstacle C_3 during the course when particle crosses them. Evidently, the particle takes more time to pass the obstacle if it collides the nearby obstacle. On the other hand, if particle passes across the obstacle without touching it then it takes less time to cross the obstacle. The fluid behavior spread across the diamond shaped obstacles controls the motion of the particle in such a way that the particle may or may not collide with the obstacle. Table 1-6 show the maximum and minimum values of drag on the diamond shaped obstacles and the time to cross obstacles with different arrangements of obstacles. t_2 and t_4 represent the time to cross obstacles C_2 and C_4 respectively. Similarly, S_2, S_3 and S_4 are the shifts attained by the particle while crossing C_2, C_3, and C_4. If the falling particle shifts towards the right side with a value greater than 2.5 or shifts towards the left side with a value less than 0.4 while passing and crossing the obstacle then it assures that the particle has collided while crossing the obstacle. In some cases the particle passes without colliding or touching the obstacle.

4. Conclusion

In this research work, we have performed numerical simulations using a direct approach and simulated the particulate flow by using FBM. We have examined the behaviour of falling particle under the action of gravitational acceleration, the collision and interaction of particle with four internal diamond shaped obstacles within a fluid flow channel. We have also discussed the behavior of obstacles. In case of four circular obstacles the first obstacle is fixed and second obstacle is placed at two different positions in negative x-direction and fourth obstacle is placed at three different positions along y-direction. A solid particle which is falling from three different positions, this particle is interacting and colliding with all the diamond shaped obstacles. The main benefit of FBM is that the Computational coarse Mesh is fixed (Eulerian) w.r.t time and less computational effort is required to pass the particle from obstacles. The diameter of the particle which is falling down and the diagonal length of the diamond shaped obstacle are same.

A specific collision model is also defined for the collision of the particle and diamond shaped obstacles. Force of collision with wall is also defined in the code of FEATFLOW. Benefit of these collision models is that it can treat the scenario when the particle interact and start to overlap with obstacles due to numerical errors. When a particle comes in the vicinity of any obstacle, the collision model gets activated and produces very promising results.

We have discussed the numerical results for a falling rigid particle crossing and passing around diamond shaped obstacles under the action of gravitational acceleration inside an incompressible fluid channel, in which a particle is allowed to fall freely from three different initial positions. We have calculated the numerical results on a fixed computational mesh with refinement level 5. We have examined the change in the behavior of fluid inside a channel when a particle starts to cross the obstacles and meanwhile interacts with them. We used different configurations for the diamond shaped obstacles (staggered and inline) to examine the fluid behavior in a channel. The numerical results are discussed in detail by calculating the max/min time t_2 to cross second obstacle, max/min time t_4 to cross fourth obstacle. We have also calculated max/min shifts s_2, s_3 and s_4 on obstacles C_2, C_3 and C_4. Drag coefficient on obstacle 1, obstacle 2 and obstacle 3 while particle crosses each of them is also presented.

References

[1] Sydney Chapman and T. G. Cowling. The mathematical theory of non-uniform gases. *American Journal of Physics*, **30**(5), 389–389 (1962).

[2] Andriy Sokolov, Ramzan Ali, and Stefan Turek. An afc-stabilized implicit finite element method for partial differential equations on evolving-in-time surfaces. *Journal of Computational and Applied Mathematics*, **289**, 101 – 115 (2015). Sixth International Conference on Advanced Computational Methods in Engineering (ACOMEN 2014).

[3] C S Campbell. Rapid granular flows. *Annual Review of Fluid Mechanics*, **22**(1), 57–90 (1990).

[4] Paul W. Cleary. Dem simulation of industrial particle flows: case studies of dragline excavators, mixing in tumblers and centrifugal mills. *Powder Technology*, **109**(1), 83 – 1042 (2000).

[5] R. Glowinski, T. W. Pan, T. I. Hesla, and D. D. Joseph. A distributed lagrange multiplier/fictitious domain method for particulate flows. *International Journal of Multiphase Flow*, **25**(5), 755 – 794 (1999).

[6] C. W Hirt, A. A Amsden, and J. L Cook. An arbitrary lagrangian-eulerian computing method for all flow speeds. *Journal of Computational Physics*, **14**(3), 227 – 253 (1974).

[7] Bertrand Maury. Characteristics ale method for the unsteady 3d navier-stokes equations with a free surface. *International Journal of Computational Fluid Dynamics*, **6**(3), 175–188 (1996).

[8] D. Wan and S. Turek. Fictitious boundary and moving mesh methods for the numerical simulation of rigid particulate flows. *Journal of Computational Physics*, **222**(1), 28 – 56 (2007).

[9] P. Singh, T. I. Hesla, and D. D. Joseph. Distributed lagrange multiplier method for particulate flows with collisions. *International Journal of Multiphase Flow*, **29**(3), 495 – 509 (2003).

[10] N. A. Patankar, P. Singh, D. D. Joseph, R. Glowinski, and T. W. Pan. A new formulation of the distributed lagrange multiplier/fictitious domain method for particulate flows. *Int. J. Multiphase Flow*, **26**, 1509–1524 (2000).

[11] Khuram Walayat, Zekun Wang, Kamran Usman, and Moubin Liu. An efficient multi-grid finite element fictitious boundary method for particulate flows with thermal convection. *International Journal of Heat and Mass Transfer*, **126**, 452 – 465 (2018).

[12] K. Usman, K. Walayat, R. Mahmood, and N. Kousar. Analysis of solid particles falling down and interacting in a channel with sedimentation using fictitious boundary method. *AIP Advances*, **8**(6), 065201 (2018).

[13] Khuram Walayat, Zhilang Zhang, Kamran Usman, Jianzhong Chang, and Moubin Liu. Dynamics of elliptic particle sedimentation with thermal convection. *Physics of Fluids*, **30**(10), 103301 (2018).

[14] Khuram Walayat, Zhilang Zhang, Kamran Usman, Jianzhong Chang, and Moubin Liu. Fully resolved simulations of thermal convective suspensions of elliptic particles using a multigrid fictitious boundary method. *International Journal of Heat and Mass Transfer*, **139**, 802 – 821 (2019).

[15] Saqia Jabeen, Kamran Usman, and Khuram Walayat. Numerical investigations for a chain of particles settling in a channel. *Computational Particle Mechanics*, Oct 2019.

[16] K Usman, K Walayat, R Mahmood, and N Kousar. Analysis of solid particles falling down and interacting in a channel with sedimentation using fictitious boundary method. *AIP Advances*, **8**(6), 065201 (2018).

[17] Khuram Walayat, Zekun Wang, Kamran Usman, and Moubin Liu. An efficient multi-grid finite element fictitious boundary method for particulate flows with thermal convection. *International Journal of Heat and Mass Transfer*, **126**, 452–465 (2018).

[18] Khuram Walayat, Zhilang Zhang, Kamran Usman, Jianzhong Chang, and Moubin Liu. Dynamics of elliptic particle sedimentation with thermal convection. *Physics of Fluids*, **30**(10), 103301 (2018).

[19] Neelesh A Patankar, Pushpendra Singh, Daniel D Joseph, Roland Glowinski, and T-W Pan. A new formulation of the distributed lagrange multiplier/fictitious domain method for particulate flows. *International Journal of Multiphase Flow*, **26**(9), 1509–1524 (2000).

[20] Ashok S Sangani and Guobiao Mo. Inclusion of lubrication forces in dynamic simulations. *Physics of fluids*, **6**(5), 1653–1662 (1994).

[21] Waqas Sarwar Abbasi, Shams-ul Islam, Hamid Rahman, and Raheela Manzoor. Numerical investigation of fluid-solid interaction for flow around three square cylinders. *AIP Advances*, **8**(2), 025221 (2018).
[22] O Inoue, M Mori, and N Hatakeyama. Aeolian tones radiated from flow past two square cylinders in tandem. *Physics of Fluids*, **18**(4), 046101 (2006).
[23] Si-ying Wang, Fang-bao Tian, Lai-bing Jia, Xi-yun Lu, and Xie-zhen Yin. Secondary vortex street in the wake of two tandem circular cylinders at low reynolds number. *Physical Review E*, **81**(3), 036305 (2010).
[24] Anthony J. C. Ladd. Numerical simulations of particulate suspensions via a discretized boltzmann equation. part 1. theoretical foundation. *Journal of fluid mechanics*, **271**, 285–309 (1994).
[25] John F Brady and Georges Bossis. Stokesian dynamics. *Annual review of fluid mechanics*, **20**(1), 111–157 (1988).
[26] Decheng Wan and Stefan Turek. An efficient multigrid-fem method for the simulation of solid-liquid two phase flows. *Journal of Computational and Applied Mathematics*, **203**(2), 561 – 580 (2007).
[27] Jianping Zhang, Liang-Shih Fan, Chao Zhu, Robert Pfeffer, and Dewei Qi. Dynamic behavior of collision of elastic spheres in viscous fluids. *Powder technology*, **106**(1-2), 98–109 (1999).
[28] Kamran Usman. *Numerical Analysis of Collision Models in 2D Particulate Flow*. PhD thesis, Technische Universitaet Dortmund, Fakultaet fuer Mathematik, 2013.
[29] P. A. Arp and S. G. Mason. The kinetics of flowing dispersions: Ix. doublets of rigid spheres (experimental). *Journal of colloid and interface science*, **61**(1), 44–61 (1977).
[30] A. M. Ardekani and R. H. Rangel. Unsteady motion of two solid spheres in stokes flow. *Physics of Fluids*, **18**(10), 103306 (2006).
[31] A. M. Ardekani and R. H. Rangel. Numerical investigation of particle-particle and particle-wall collisions in a viscous fluid. *Journal of Fluid Mechanics*, **596**, 437–466 (2008).
[32] Suhas Patankar. *Numerical heat transfer and fluid flow*. CRC press, 2018.
[33] Stefan Turek, Decheng Wan, and Liudmila S Rivkind. The fictitious boundary method for the implicit treatment of dirichlet boundary conditions with applications to incompressible flow simulations. In *Challenges in Scientific Computing-CISC 2002*, Springer, pages 37–68 (2003).
[34] Stefan Turek. *Numerical Analysis of a New Time-stepping θ-scheme for Incompressible Flow Simulations.* Ergebnisberichte angewandte Mathematik. Univ. Dortmund, Fachbereich Mathematik, 2005.
[35] Decheng Wan and Stefan Turek. Direct numerical simulation of particulate flow via multigrid fem techniques and the fictitious boundary method. *International Journal for Numerical Methods in Fluids*, **51**(5), 531–566 (2006).
[36] Decheng Wan, Stefan Turek, and Liudmila S. Rivkind. An efficient multigrid fem solution technique for incompressible flow with moving rigid bodies. In Miloslav Feistauer, Vit Dolejsi, Petr Knobloch, and Karel Najzar, editors, *Numerical Mathematics and Advanced Applications*, pages 844–853. Springer Berlin Heidelberg, 2004.
[37] S. Kim and S.J. Karrila. *Microhydrodynamics: Principles and Selected Applications*. Butterworth - Heinemann series in chemical engineering. Dover Publications, 2005.
[38] S. Turek. Featflow. finite element software for the incompressible navier-stokes equations: User manual, release 1.1. Technical report, 1998.
[39] K. Walayat, Z. Wang, K. Usman and M. Liu. *A multigrid finite element fictitious boundary method for fluid-solid two-phase flows*. The 8th International Conference on Computational Methods. ScienTech Publisher, 2017.
[40] Jianming Yang and Frederick Stern. A non-iterative direct forcing immersed boundary method for strongly-coupled fluid-solid interactions. editors, *Journal of Computational Physics*, pages 779–804 (2015).
[41] Cleary, PW. Discrete element modelling of industrial granular flow applications. *TASK. Quarterly-Scientific Bulletin*, 385–416 (1998).
[42] Glowinski, Roland and Pan, Tsorng-Whay and Periaux, Jacques. Distributed Lagrange multiplier methods for incompressible viscous flow around moving rigid bodies. *Computer methods in applied mechanics and engineering*, 181–194 (1998).
[43] Glowinski, Roland. Finite element methods for incompressible viscous flow. *Handbook of numerical analysis*, 3–1176 (2003).